Available online at www.sciencedirect.com
ScienceDirect
International Journal of Heat and Mass Transfer 50 (2007) 1018–1034
International Journal of HEAT and MASS TRANSFER
www.elsevier.com/locate/ijhmt

Boiling heat transfer in a hydrofoil-based micro pin fin heat sink

Ali Koşar, Yoav Peles *

Department of Mechanical, Aerospace and Nuclear Engineering, Rensselaer Polytechnic Institute, Troy, NY 12180, USA

Received 1 May 2006
Available online 23 October 2006

Abstract

Flow boiling of R-123 in a hydrofoil-based micro pin fin heat sink was investigated. Average two-phase heat transfer coefficients were obtained over effective heat fluxes ranging from 19 to 312 W/cm^2 and mass fluxes from 976 to 2349 kg/m^2 s. The paper presents a flow map, which divides the data into three flow pattern regions: bubbly, wavy intermittent and spray-annular flows. Heat transfer coefficient trends and flow morphologies were used to infer boiling heat transfer mechanisms. Existing conventional scale correlations for circular tubes resulted in large scatter and were not able to predict the heat transfer coefficients accurately.

Keywords: Pin fin; Microchannels; Cross-flow; Flow pattern; MEMS; Boiling

1. Introduction

Research concerning heat transfer in microsystems has been growing rapidly in the last decade. As part of this endeavor, single-phase flows [1–10] and boiling flows [11–28] have been topics of great interest. Initial studies were dedicated to reveal the thermal and hydrodynamic characteristics of microchannel flows, but recently emerging reports extend this effort to other configurations like pin fins [29–35]. The pin fin shapes employed in these studies were primarily adopted from conventional scale heat sinks like circular [36,37], square [38], diamond [39], and rectangular [40].

Single-phase flow over pin fin heat sinks has been extensively investigated over the years [41–44] and is still a topic of active research [45–57]. Since boiling is often a desired heat transfer mode, it has also been visited in the context of fins. Pin fins are commonly used to enhance pool boiling heat transfer, and various studies have been performed in conventional scale to provide knowledge concerning the boiling phenomenon [58–73]. Honda and co-workers in several recent publications [74–76] utilized successfully micro pin fins to augment the critical heat flux (CHF) conditions in electronic components.

In conventional scale, cross-flow boiling over circular tube bundles has been meticulously studied; collected data and correlations pertaining to large scale systems are available in numerous archival publications [77–100]. Onset of nucleate boiling [78,79], heat transfer coefficients [80–89], critical heat flux conditions [90–94], pressure drop [95–98], and flow morphologies [99,100] have been obtained and correlated, mainly for circular tube bundles. For example, Jensen and Hsu [81] conducted a parametric study of boiling heat transfer in a horizontal tube bundle and reported an increase in local heat transfer coefficient with increasing heat flux, pressure and mass velocity, but found the effect of quality to be minor. Gupta et al. [84] and Gupta [89] studied the effects of heat flux, mass velocity, and tube geometry on local boiling heat transfer of water in small horizontal tube bundles at low velocities. However, the data presented by them were limited to low mass velocities (<9 kg/m^2 s). Chen-type heat transfer coefficient

* Corresponding author. Tel.: +1 518 276 2886; fax: +1 518 276 2623.
E-mail address: pelesy@rpi.edu (Y. Peles).

0017-9310/$ - see front matter © 2006 Elsevier Ltd. All rights reserved.
doi:10.1016/j.ijheatmasstransfer.2006.07.032

Nomenclature

a_1, a_2, a_3 parameters in correlation 8
A_b base area (surface area without pin fins), m^2
$A_{c,fin}$ fin cross-sectional area, m^2
A_{fin} total fin surface area, m^2
A_{min} minimum cross-sectional area, m^2
A_p planform area (surface area of silicon block), m^2
A_t total heat transfer area ($A_b + \eta_f A_{fin}$), m^2
b_1, b_2, b_3, b_4 constants in correlation 9
Bo Boiling number based on q''_w, $Bo = q''_w/(Gh_{FG})$
Bo_{ch} Boiling number based on the average mass velocity, $Bo_{ch} = q''_w/(G_{av}h_{FG})$
c_p specific heat at constant pressure, kJ kg^{-1} $°C^{-1}$
Cor correction factor in correlation 6
d chord thickness, m
d_h channel hydraulic diameter, m
E enhancement factor
f_f friction factor
F two-phase Reynolds number factor
g gravitational constant, m s^{-2}
G mass velocity based on the minimum cross-sectional area, kg m^{-2} s^{-1}
G_{av} mass velocity based on the entire cross-sectional area, kg m^{-2} s^{-1}
h_{FG} latent heat of vaporization, J kg^{-1}
$\bar{h}_{sp}$ average single-phase heat transfer coefficient at a definite flow rate, W m^{-2} $°C^{-1}$
$\bar{h}_{tp}$ average two-phase heat transfer coefficient at a definite flow rate, W m^{-2} $°C^{-1}$
H channel height, fin height, m
h_{av} average heat transfer coefficient at a definite heat flux, W m^{-2} $°C^{-1}$
j_G superficial gas velocity, Gx/ρ_G, m s^{-1}
j_L superficial liquid velocity, $G(1-x)/\rho_L$, m s^{-1}
k_{fin} thermal conductivity of the fin (silicon), W m^{-1} $°C^{-1}$
k_{fluid} thermal conductivity of the fluid, W m^{-1} $°C^{-1}$
k_s thermal conductivity of the silicon block, W m^{-1} $°C^{-1}$
L channel length, m
m constant
M number of data points at a fixed mass velocity
$\dot{m}$ mass flow rate, kg s^{-1}
m_f fin parameter in Eq. (2)
M_t total number of data points
MAE mean absolute error
N_{column} number of pin fins in a single column
N_{row} number of pin fins in a single row
N_t total number of pin fins
Nu Nusselt number
Nu_{ch} Nusselt number based on the channel hydraulic diameter
$\overline{Nu}$ average Nusselt number at a definite Reynolds number
Nu_{av} average Nusselt number at a definite heat flux
P electrical power, W
p_e exit pressure, kPa
P_{fin} pin fin perimeter, m
Pr Prandtl number
q'' effective heat flux, W cm^{-2}
q''_w heat flux based on the heat transfer surface area of the device, W cm^{-2}
$\dot{Q}_{loss}$ heat loss, W
R electrical resistance, Ω
Re Reynolds number based on the chord thickness, $Re = Gd/\mu$
Re_{ch} Reynolds number based on the channel hydraulic diameter, $Re_{ch} = G_{av}d_h/\mu$
S suppression factor
S_L longitudinal pitch, m
S_T transverse pitch, m
t thickness of the silicon block, m
T temperature, °C
$\overline{T}$ average surface temperature, °C
T_e exit temperature, °C
$\overline{T}_{heater}$ average heater surface temperature °C
T_i inlet temperature, °C
U quantity under consideration
W channel width, m
x mass quality
x_e exit mass quality
X_o bubble growth parameter, m
X_{vt} Martinelli parameter
We Weber number, $We = G^2d/(\sigma\rho)$
We_{ch} Weber number based on the channel hydraulic diameter, $We_{ch} = G_{av}^2 d_h/(\sigma\rho)$

Greek symbols
β aspect ratio
η_f fin efficiency
ϕ_L^2 two-phase friction multiplier
μ viscosity, kg m^{-1} s^{-1}
ρ density, kg m^{-3}
σ surface tension, N m^{-1}

Subscripts
amb ambient
av average
ch channel
CHF critical heat flux
e exit
f fluid
fin fin
G gas
i inlet
j index in Eqs. (3) and (4)
L liquid

LO	liquid only	se	surface at the end of the single-phase length
mic	microconvection	si	surface at the inlet
nb	nucleate boiling	tp	two-phase
s	surface	v	vapor
sat	saturation		

models were successfully employed in these studies to correlate the experimental data. Dowlati et al. [86] reported agreement between boiling heat transfer coefficients of R-113 and existing pool boiling correlations, and attributed the conformity to the dominance of nucleate boiling heat transfer mechanism.

In boiling heat transfer studies, heat transfer coefficients have been shown to be closely related to the flow patterns. Grant and Chisholm [99] reviewed studies about flow patterns and pressure drop of air–water two-phase flow on the shell-side of segmentally baffled shell- and tube-heat exchangers. They reported spray, bubbly, intermittent, stratified-spray, and stratified flow patterns. A flow map was then constructed based on the superficial velocities of each phase. Noghrehkar et al. [100] extended the work of Grant and Chisholm [99]. They studied flow patterns in two-phase flow across a tube bundle under adiabatic conditions and identified bubbly, intermittent and annular flows, and also developed a flow map with the use of liquid and gas superficial velocities.

Flow patterns also have a vital role in determining the CHF mechanism. Leroux and Jensen [93] investigated upward vertical cross-flow of R-113 in horizontal tube bundles. They studied the effects of mass flux, quality, pressure, and bundle geometry on CHF conditions and found three distinct curve trends, which were linked to flow patterns and distinct CHF mechanisms. Bubbly flow was present at low qualities and mass velocities, and the CHF conditions were triggered by departure from nucleate boiling (DNB), while at high qualities and mass velocities, in which spray-annular flow was dominant, the CHF was a result of dryout.

The existing scientific data about flow boiling over tube bundles in conventional scale gathered over the years provide an excellent knowledge base, which can be exploited while studying the phenomena at diminishing length scale. However, before this can be done, there are several key issues that need to be addressed. Extending the limited scaling laws of boiling to microscale is not fully understood even for the more rudimentary channel flow geometry. Extensive research effort to unveil these scaling laws for microchannels is still underway. Although literature concerning boiling cross-flow over pin fins is available, these flow configurations are less explored compared to channel flow. Furthermore, microfabrication technology enables the formation of pin fin geometries with enhanced thermal-hydraulic performance, which are often uneconomical to form by standard macro scale technology. The available data for unconventional geometries is therefore very limited.

This article reports an experimental study of R-123 flow boiling over a hydrofoil-based micro pin fin heat sink and aims at evaluating boiling heat transfer coefficients, flow patterns, and heat transfer mechanisms. Additionally, results have been compared with existing correlations developed for circular conventional scale pin fins. Finally, modified heat transfer coefficient correlations, a flow map, and boiling map are proposed based on the experimental data obtained in the current experiments.

2. Device overview and microfabrication process flow

2.1. Device overview

A computer aided design (CAD) schematic of the device consisting of a 1800 μm wide and 1 cm long microchannel of depth 243 μm is shown in Fig. 1. The microchannel contains 20 arrays of 12 and 13 (in tandem) staggered NACA 66-021 hydrofoil pin fins with a wetted perimeter of 1030 μm and chord thickness of 100 μm. In order to minimize ambient heat losses an air gap is formed on the two ends of the side walls, and an inlet and exit plenum, 4 mm long each, are etched on the thin silicon substrate (∼150 μm). A heater, which serves as a thermistor for temperature measurements, is deposited on the backside under the pin fin arrays to deliver the heating power. A Pyrex cover seals the device from the top and allows flow visualization. Pressure taps are placed at the inlet and exit of the device to enable pressure measurements.

2.2. Microfabrication process flow

A double side polished, n-type ⟨1 0 0⟩ single crystal silicon wafer is processed on both sides to create a MEMS device, which consists of a microchannel enclosing an array of fins. In the fabrication process first, the top side and bottom side masks are designed and fabricated. A 1 μm thick oxide is deposited on both sides of the silicon wafer to protect the bare wafer surface. The heater and the vias are formed on the backside of the wafer by cryopumped CVC 601 sputter deposition system. A 70 Å thick layer of titanium is initially deposited to enhance adhesion characteristics and is followed by sputtering a 1 μm thick layer of aluminum containing 1% silicon and 4% copper. Subsequent photolithography and concomitant wet bench processing create the heater on the backside of the wafer. Next, the microchannel with micro pin fins is formed on the top side of the wafer. For this, the wafer is

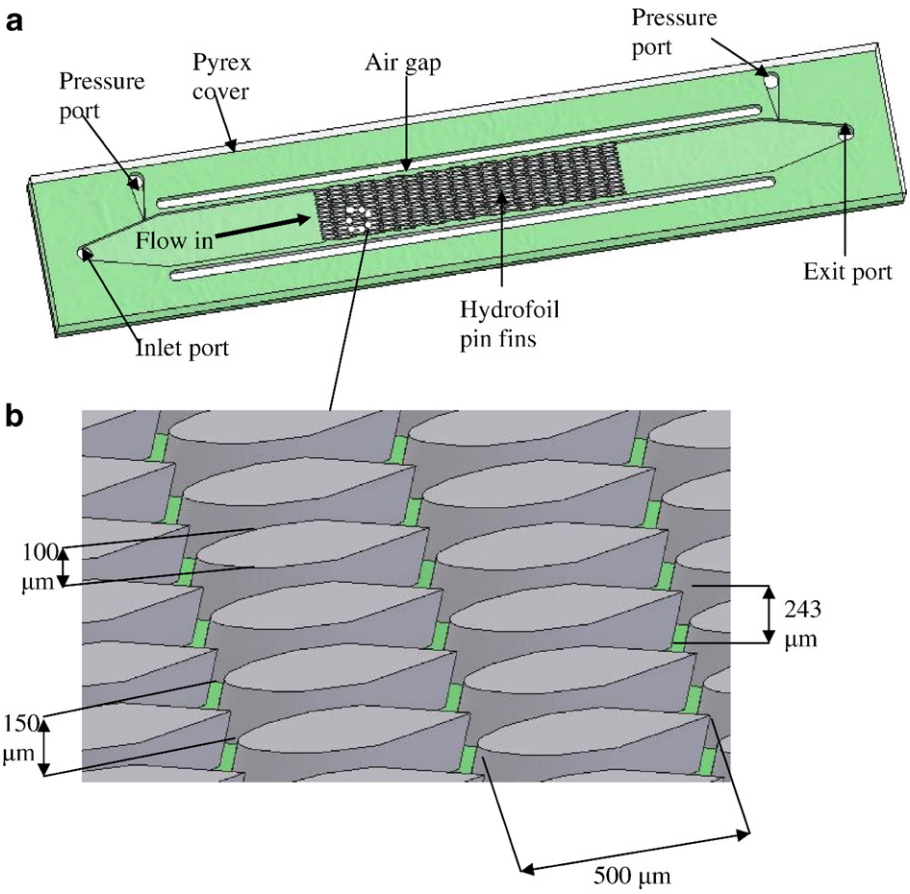

Fig. 1. (a) CAD model of the micro pin fin heat sink. (b) Zoom in to the micro pin fins.

taken through a photolithography step and a reactive ion etching (RIE) oxide removal process to mask certain areas on the wafer, which are not to be etched during the deep reactive ion etching (DRIE) process. The wafer is consequently etched in a DRIE process, and silicon is removed from places not protected by the photoresist/oxide mask. The DRIE process forms deep vertical trenches on the silicon wafer with a characteristic scalloped sidewall possessing a peak-to-peak roughness of ~0.3 μm. A profilometer and an SEM are employed to measure and record various dimensions of the device. The wafer is flipped and the backside is then processed, so that an inlet, exit, side air gap, and pressure port taps for the transducers are formed. A photolithography followed by a buffered oxide etch (BOE) (6:1) oxide removal process is carried out to create a pattern mask. The wafer is then etched-through in a DRIE process to create the fluidic ports. Thereafter, electrical contacts/pads are opened on the backside of the wafer by performing another round of photolithography and RIE processing. Finally, the processed wafer is stripped of any remaining resist or oxide layers and anodically bonded to a 1 mm thick polished Pyrex (glass) wafer to form a sealed device. After successful completion of the bonding process, the processed stack is die-sawed to separate the devices from the parent wafer.

3. Experimental setup and procedure

3.1. Experimental setup

The experimental setup used in present study is shown in Fig. 2. The micro pin fin device was packaged in between two plates. The fluidic seals were forged using miniature "o-rings" while external electrical connections to the heater were provided from beneath through spring-loaded pins, which connected the heater to electrical pads residing away from the main micro pin fin device body. Resistance of the heater and pressure drop were recorded for different flow rates in the loop. The electrical power was supplied to the device with an INSTEK programmable power supply, and electrical current and voltage were measured using a HP3457A digital multimeter. A 180 Series Micropump annular gear pump capable of generating flowrates from 0.3 to 145 ml/min was used to propel the liquid from a reservoir through the MEMS device at various flow rates, and the inlet temperature was measured by an Omegaette HH308 type K thermometer. Inlet and exit pressures were measured via pressure transducers. Flow rate measurements were made using Omega FL-111 flow meter. Pressure and flow rates were acquired together with the voltage and current for data reduction. The flow was visualized with a Leica DMLM microscope, and flow images

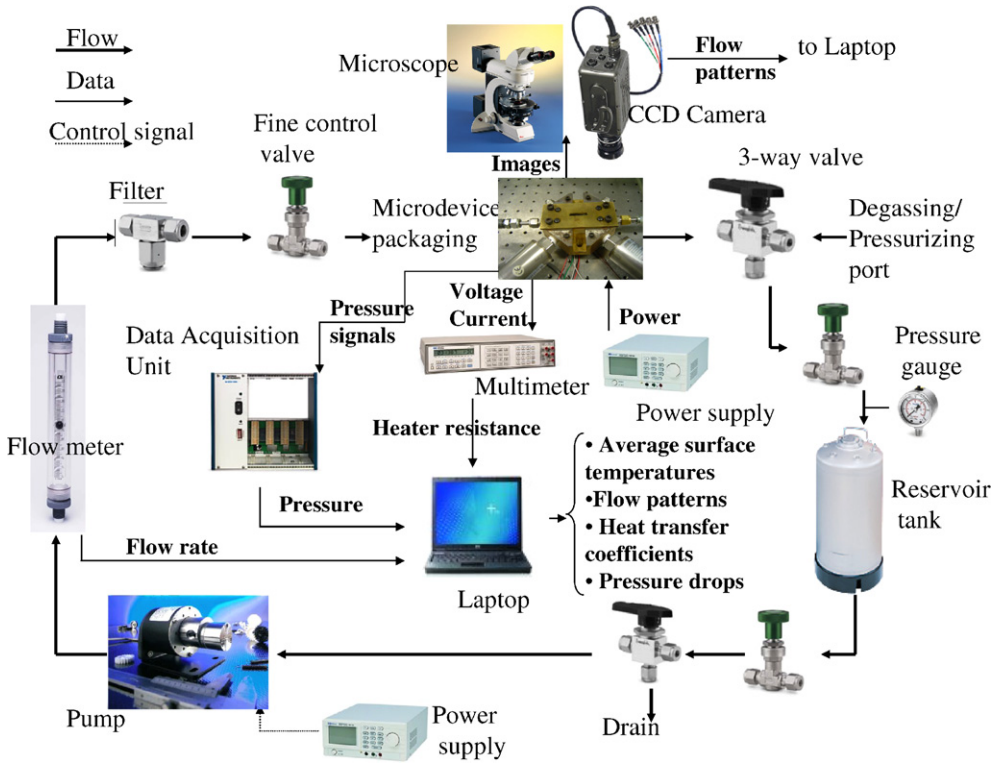

Fig. 2. Experimental setup with flow, data, and control signal directions.

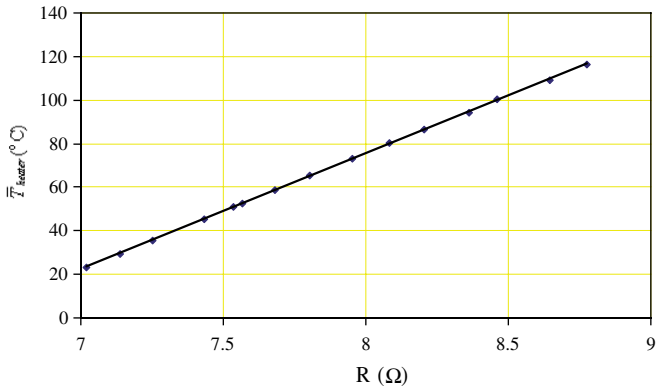

Fig. 3. Average temperature as a function of electrical resistance (temperature calibration curve).

were taken via a Vision Research Phantom V-4 series high-speed camera capable of capturing frames with a rate up to 90,000 frames per second, a maximum resolution of 512×512 pixels, and a minimum exposure time of 2 μs. Flow visualization was performed to scrutinize the boiling flow patterns along the entire micro pin fin device and to measure the single-phase length L_{sp}, which is the distance from the inlet to the location of first appearance of boiling.

3.2. Experimental procedure

R-123 was utilized as the working fluid in the experiments under exit pressures of 486–539 kPa. Before starting the experiment, the device was calibrated in a well insulated and temperature controlled oven to obtain the heater electrical resistance-temperature linear calibration curve (Fig. 3). This calibration curve was used to obtain the average surface temperature of the device during the data reduction process. A standard deviation of 0.15 °C was obtained between the individual data points and the calibration curve.

In order to estimate heat losses, electrical power was applied to the test section after evacuating the working fluid from the test loop. Once the temperature of the test section reached steady-state conditions, the temperature difference between the ambient and test section was recorded at the corresponding power. The temperature difference versus power curve was plotted and used to compare the heat loss associated with each experimental data point to the fin analysis. The measured heat losses were subtracted from the total heats supplied to the heat sink under forced flow conditions, and the corresponding values were used in subsequent analysis of the data reduction.

The experiments were performed under steady state conditions, and the inlet temperature was held constant at ambient temperature for all data points. Firstly a steady flow was acquired by setting the flow meter at a desired value. The exit pressure was kept at a constant value for all the experiments. An increase in the inlet pressure was recorded as the heat flux increased during flow boiling, and average pressure difference between the inlet and exit pressures was used to evaluate the saturation temperature. However, since the increase in the average pressure was less

compared to the inlet pressure, the saturation temperature was not affected much by the change in the inlet pressure. Prior to acquiring experimental data the electrical resistance of the heater was measured at room temperature. The flow meter reading was adjusted to the desired flow rate, and the pressure difference between the inlet and exit pressure ports was recorded through a LabView® interface to a spreadsheet file. To obtain heat transfer data, voltage was applied in 0.5 V increments across the heater, and the current/voltage data were recorded while keeping the flow rate constant. At impending CHF condition a slight increase in the applied power causes an abrupt surge of the wall temperature. The power was switched off when this condition was reached. The same procedure was repeated for all the flow rates.

4. Data reduction

4.1. Single-phase heat transfer

Data obtained from the voltage, current and pressure measurements were used to calculate the average single- and two-phase temperatures, Nusselt numbers, and single- and two-phase heat transfer coefficients. The electrical input power and heater resistance were determined using the measured voltage and current values, respectively. Thereafter, the heater electrical resistance-temperature calibration curve was used for determining the average heater temperature. The surface temperature at the base of the microchannels was then calculated as

$$\overline{T} = \overline{T}_{\text{heater}} - \frac{(P - \dot{Q}_{\text{loss}})t}{k_s A_p} \tag{1}$$

The heat transfer coefficient was obtained using Newton's law of cooling jointly with the 1-D steady-state adiabatic tip fin equation as follows:

$$(P - \dot{Q}_{\text{loss}}) = h_{\text{av}}(\eta_f N_t P_{\text{fin}} H + wL - N_t A_{c,\text{fin}})\left[\overline{T} - \left(\frac{T_i + T_e}{2}\right)\right] \tag{2}$$

where $\eta_f = \frac{\tanh(m_f H)}{m_f H}$, $T_e = T_i + \frac{P - \dot{Q}_{\text{loss}}}{\dot{m} c_p}$, and $m_f = \sqrt{\frac{h_{\text{av}} P_{\text{fin}}}{k_{\text{fin}} A_{c,\text{fin}}}}$.

The transcendental equation (2) was solved iteratively to obtain h_{av}.

An average value of the heat transfer coefficient and Nusselt number for a fixed Reynolds number was then calculated as shown below

$$\bar{h} = \frac{1}{M}\sum_{j=1}^{M}(h)_{\text{av},j} \tag{3}$$

$$\overline{Nu} = \frac{1}{M}\sum_{j=1}^{M}(h_{\text{av}})_{\text{av},j}\frac{d}{k_{\text{fluid}}} \tag{4}$$

4.2. Boiling heat transfer

Under boiling conditions, the microchannels are divided into two length regions: single-phase (L_{sp}), and two-phase (L_{tp}), which are obtained by flow visualization. The single-phase length L_{sp} was defined as the distance between the inlet of microchannels and the location of first active nucleation sites detected on the micro pin fin surface, while the two-phase length L_{tp} is the difference between the microchannel length and the single-phase length. Using 1-D fin analysis with the assumption of adiabatic tip $\bar{h}_{\text{tp}}$ can be expressed as follows:

$$(P - \dot{Q}_{\text{loss}}) = \bar{h}_{\text{tp}}(\eta_f N_t P_{\text{fin}} H + wL - N_t A_{c,\text{fin}})[\overline{T_{\text{tp}}} - T_{\text{sat}}] \tag{5}$$

The surface temperatures at the inlet and the first appearance of flow boiling are given as

$$T_{\text{si,sp}} = T_i + \frac{q''_w}{\bar{h}_{\text{sp}}} \tag{6}$$

$$T_{\text{se,sp}} = T_{\text{sat}} + \frac{q''_w}{\bar{h}_{\text{sp}}} \tag{7}$$

The average surface temperature in the single-phase region is the mean surface temperature

$$\overline{T}_{\text{sp}} = \frac{T_{\text{si,sp}} + T_{\text{se,sp}}}{2} \tag{8}$$

With $\overline{T}_{\text{sp}}$ known, $\overline{T}_{\text{tp}}$ is obtained from a weighted average of the single and two-phase regions surface temperatures

$$\overline{T}_{\text{tp}} = \frac{\overline{T}L - \overline{T}_{\text{sp}}L_{\text{sp}}}{L_{\text{tp}}} \tag{9}$$

Finally, the exit quality can be calculated with the known mass flow rate and net power supplied to the device as

$$x_e = \frac{(P - \dot{Q}_{\text{loss}}) - \dot{m} c_p (T_{\text{sat}} - T_i)}{\dot{m} h_{FG}} \tag{10}$$

In the current study, the mass velocity was fixed for a given exit pressure.

Mean absolute error (MAE) is used to compare the experimental results with various correlations according to the following expression:

$$\text{MAE} = \frac{1}{M_t}\sum_{i=1}^{M_t}\frac{|U_{\text{exp}} - U_{\text{theoretical}}|}{U_{\text{exp}}}100\% \tag{11}$$

The uncertainties of the measured values are obtained from the manufacturer's specification sheets, while the uncertainties of the derived parameters are calculated using the method developed by Kline and McClintock [101]. Uncertainties in the flow rate, average surface temperature, single-phase and two-phase convective heat transfer coefficients are estimated to be 1%, 0.5 °C, 5% and 6.8%, respectively.

5. Results and discussion

The average surface temperature as a function of the heat flux at three different mass velocities is depicted in Fig. 4. During single-phase flow the curves are linear, which is typical of single-phase heat transfer at constant heat flux. However, the slopes decrease with mass velocity since the flow temperature diminishes with increasing flow rate. Once boiling is triggered at the exit, a partial boiling region is established. With an increase in heat flux, the boiling region expands to upstream until it encompasses the entire flow domain, and the two-phase flow is said to be fully developed. The three different regions (single-phase, partial and fully developed boiling flow) are characterized by different heat flux-surface temperature slopes. The transition from the onset of nucleate boiling to fully developed boiling flow occurs over a limited range of heat flux. During the two-phase flow, the surface temperature continues to increase with heat flux. As the heat flux is further increased, an abrupt surge in the surface temperature occurs with a slight rise of heat flux, indicating the emergence of CHF conditions.

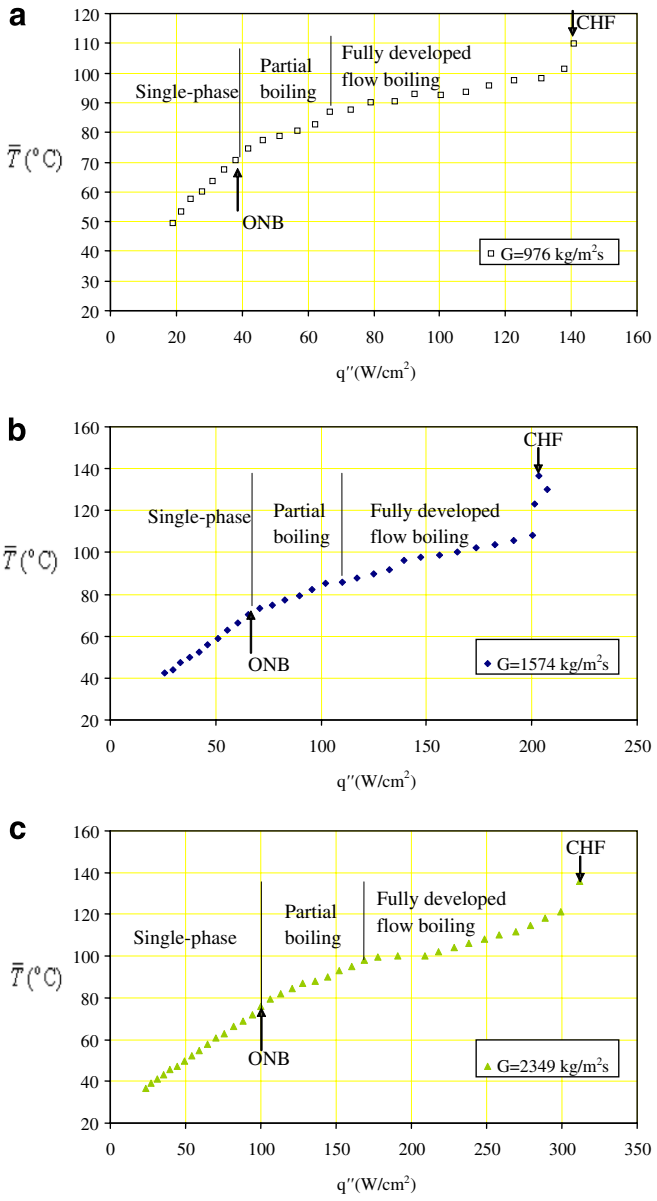

Fig. 4. Average surface temperature as a function of heat flux.

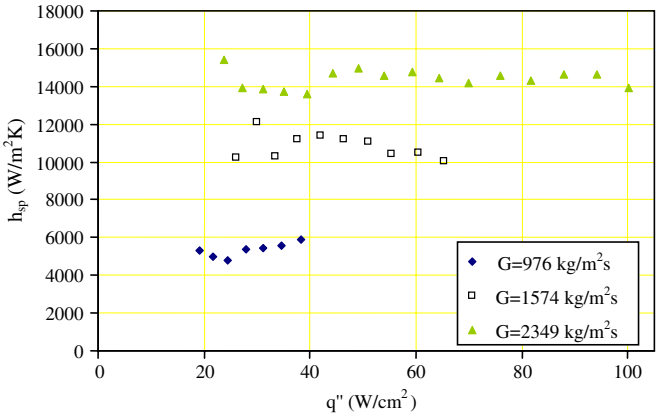

Fig. 5. Single-phase heat transfer coefficients.

The average single-phase heat transfer coefficients vary from 4800 W/m^2 K for $G = 972$ kg/m^2 s to 15,400 W/m^2 K at $G = 2349$ kg/m^2 s as shown in Fig. 5. It can be observed that the average heat transfer coefficient is strongly dependent on the mass velocity (Fig. 5) and changes little with heat flux. This is characteristic of flow across pin fins in conventional scale systems, as evidenced by the frequent use of the functional dependency of the Nusselt number on the Reynolds number ($Nu \propto Re^m$, where $0 < m < 1$ [30–57]). Concurring with conventional scale methods, the average Nusselt number is represented as a function of the Reynolds number with the following best curve fit correlation, which provides the following expression with an MAE of 5%:

$$\overline{Nu} = 0.24Re^{0.75} - 8.88 \tag{12}$$

It should be noted that the above equation is not intended to provide a generic prediction correlation, but merely a mechanistic means to aid the evaluation of the two-phase heat transfer coefficient presented in subsequent sections.

It is interesting to note that fin efficiencies are estimated to be between 94% and 98% for single-phase flow conditions, whereas it is between 80% and 93% for boiling flow conditions. Due to the high fin efficiency values, fins significantly increase the heat transfer area and contribute to heat transfer enhancement.

5.1. Boiling heat transfer

Fig. 6 shows the two-phase heat transfer coefficient as a function of heat flux. The heat transfer coefficient increases with heat flux, reaches a maximum and then monotonically

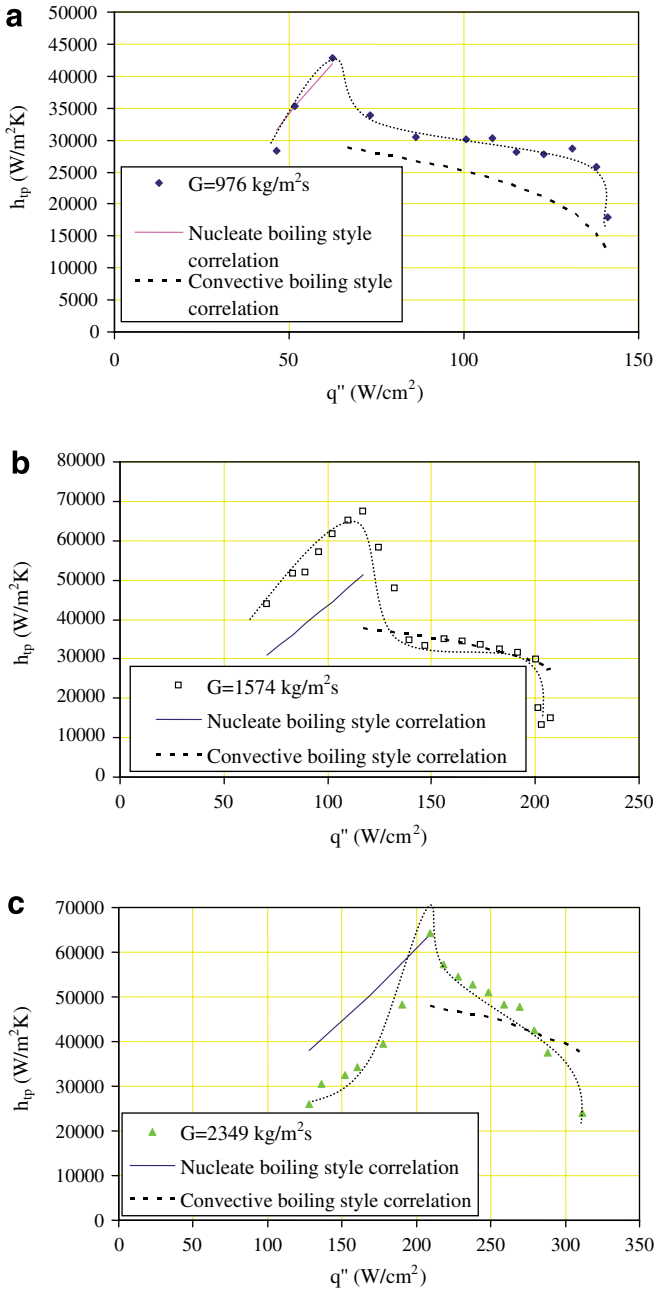

Fig. 6. Two-phase heat transfer coefficients as a function of heat flux with the predictions of Eqs. (16) and (17).

declines. Once the CHF condition is reached, the heat transfer coefficient rapidly drops. The increase in the two-phase heat transfer coefficient with heat flux has been reported in numerous tube bundle studies [78,79,84,86–90]. However, the decreasing trend after a certain maximum has not been frequently reported before.

Conventional scale flow boiling correlations for flow over tube bundles generally fall into two categories, the Chen-type correlations [102,103] used by [81,84,87,89]

$$h_{tp} = Sh_{nb} + Fh_{sp} \tag{13}$$

and the asymptotic correlations used by [88]

$$h_{tp} = \left(h_{nb}^{n} + h_{sp}^{n}\right)^{1/n} \tag{14}$$

In the Chen-type correlations the contributions of nucleate boiling and convective boiling are additive, where S and F factors are the suppression factor and two-phase convection multiplier, respectively. The single-phase heat transfer coefficient is found using existing correlations like Zukauskas [36], while the nucleate boiling heat transfer coefficient is typically obtained through a power law relation [22,86,104–108]

$$h_{nb} = Aq''^{b}_{w} \tag{15}$$

Since h_{nb} increases with heat flux, h_{tp} is expected to be strongly dependent on heat flux, when the heat transfer mechanism is predominantly nucleate boiling. The experimental data in cross-flow generally follow this trend [78,80,81,84,86,89].

The dependence of h_{tp} on mass quality has not been emphasized in previous studies [78,80,81,84,89], perhaps because the working conditions were mostly restricted to a limited range of low mass qualities ($x < 0.36$). The increasing trend of the current experimental data is in agreement with the literature at low qualities ($x < 0.2$, $x < 0.3$, $x < 0.4$ for $G = 976$, 1574, and 2349 kg/m^2 s, respectively) and generally concur with nucleate boiling dominant flow (Fig. 7). The continuous decline with heat flux at higher qualities has been also reported for boiling in microchannels for water [12,14,19,21,22] as well as refrigerant [24]. Several of these studies suggest that this characteristic trend is closely linked with convective boiling mechanism [14,21,24], while others suggest that this characteristic trend is unique to boiling flow in the micro domain [12,19]. All of this was argued in the context of microchannel boiling flow. The spray-annular flow pattern observed at high quality supports convective boiling mechanism (also see Section 5.3).

For completeness, a comparison detailing deviations and similarities in boiling heat transfer trends among plain microchannels, enhanced surface microchannels, the current configuration, and conventional scale tube bundles is included in Table 1.

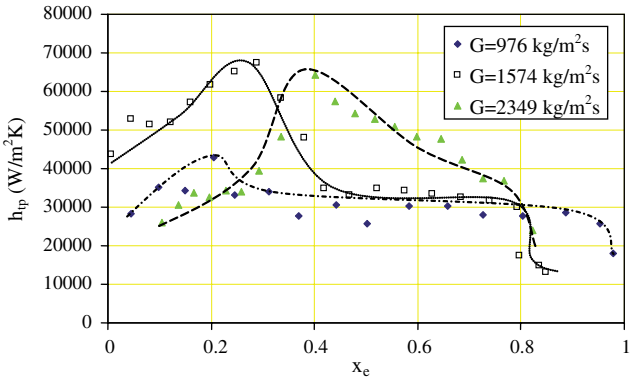

Fig. 7. Two-phase heat transfer coefficients as a function of exit quality.

Table 1
Major trends in boiling heat transfer with important parameters in microchannels, conventional tube bundles, microchannels with enhanced surfaces, and the current study

Configuration	G	q''	x_e	Flow pattern
Microchannels	h_{tp} is weakly dependent on G (slight increase) for nucleate boiling, but strongly dependent (increasing trend) for convective boiling	Strong dependence for nucleate boiling ($h_{tp} \propto q''^{const.}$), weak dependence on q'' for convective boiling	h_{tp} is weakly dependent (increasing trend) on x_e for nucleate boiling and has a moderate dependence (decreasing trend) for convective boiling	Nucleate boiling: bubbly and confined bubble Convective boiling: annular
Conventional tube bundles (circular shape)	h_{tp} moderately increases with G	h_{tp} strongly increases with q''	h_{tp} is weakly dependent on x_e (increasing trend)	Bubbly (low qualities), intermittent, annular (high qualities)
Microchannels with enhanced surfaces	At low G, nucleate boiling is dominant, and heat transfer coefficient is weakly dependent on G	h_{tp} strongly increases with$q''$for nucleate boiling	h_{tp} increases with x_e for nucleate boiling	Nucleate boiling: bubbly and confined bubble
	At high G, convective boiling is dominant, and heat transfer coefficient strongly increases with G	h_{tp} is weakly dependent on q'' for convective boiling	h_{tp} monotonically decreases with x_e for convective boiling	Convective boiling: annular
Current study	h_{tp} is moderately dependent on G	h_{tp} is strongly dependent on q'' (increasing trend) at low heat fluxes and has a weaker dependency and a decreasing trend at high heat fluxes	h_{tp} is strongly dependent on x_e (increasing trend) at low exit qualities and has a weaker dependency and a decreasing trend at high exit qualities	Low heat fluxes and exit qualities (bubbly flow pattern) Moderate heat fluxes and exit qualities (Wavy intermittent flow pattern) High heat fluxes and exit qualities (Spray-annular flow)

Table 2
Two-phase heat transfer coefficient correlations

Correlation number	Reference	Shape and geometry of pin fins, working fluid	Working fluid	Correlation
1	Hwang and Yao [78]	Circular, horizontal, staggered, $S_L/d = S_T/d = 1.5$, $G = 132$–242 kg/m^2 s, $0 < x < 0.05$	R-113	$h_{tp} = 0.2086 q''^{0.75}_w$
2	Hsu [80]	Circular, horizontal, in-line $S_L/d = S_T/d = 1.3$, $G = 50$–675 kg/m^2 s, $0 < x < 0.36$	R-113	$h_{tp} = Fh_{sp} + Sh_{nb}$ h_{sp} = experimental average single-phase heat transfer coefficient $h_{nb} = 0.5261 q''^{0.5353}_w$, $S = \left(\frac{k_L}{Fh_{sp}X_o}\right)\left(1 - \exp\left(-\frac{Fh_{sp}X_o}{k_L}\right)\right)$ $F = (\phi_L^2)^{\frac{m}{2-n}}$, $m = 0.694$, $n = 0.674$ $X_o = 0.041\left(\frac{\sigma}{g(\rho_L - \rho_v)}\right)^{0.5}$
3	Gupta et al. [84]	Circular, horizontal, in-line $S_L/d = 1.5$, $G = 0$–10 kg/m^2 s	Water	$h_{tp} = Eh_{sp} + h_{mic}$ h_{sp} = experimental average single-phase heat transfer coefficient $h_{mic} = 13.035\left(S\left(\overline{T_{tp}} - T_{sat}\right)\right)^{2.881}$, $S = \left(\frac{k_L}{Eh_{sp}X_o}\right)\left(1 - \exp\left(-\frac{Fh_{sp}X_o}{k_L}\right)\right)$ $X_o = 0.041\left(\frac{\sigma}{g(\rho_L - \rho_v)}\right)^{0.5}$, $E = 851.38 Bo^{0.707}\left(\frac{S_L}{d}\right)^{-0.245} N_{row}^{0.577}$
4	Dowlati et al. [86]	Circular, horizontal, in-line $S_L/d = S_T/d = 1.3$, $G = 50$–970 kg/m^2 s, $0 < x < 0.3$	R-113	$h_{tp} = 0.41 q''^{0.58}_w$
5	Gupta [89]	Circular, horizontal, in-line $S_L/d = 1.5$, $G = 0$–10 kg/m^2 s	Water	$h_{tp} = Eh_{sp} + h_{mic}$ h_{sp} = experimental average single-phase heat transfer coefficient $h_{mic} = 13.035\left(S\left(\overline{T_{tp}} - T_{sat}\right)\right)^{2.881}$, $S = \left(\frac{k_L}{Eh_{sp}X_o}\right)\left(1 - \exp\left(-\frac{Fh_{sp}X_o}{k_L}\right)\right)$ $X_o = 0.041\left(\frac{\sigma}{g(\rho_L - \rho_v)}\right)^{0.5}$, $E = 134.24 Bo^{0.469}\left(\frac{S_L}{d}\right)^{-0.311} \frac{N_{row}^{0.946}}{1.946} \frac{N_{column}^{0.304}}{1.304}$
6	Lee and Mudawar [24]	Rectangular, microchannels, 231 μm × 713 μm, $L = 0.0243$ m, $G_{av} = 127$–624 kg/m^2 s, $0.05 < x < 0.55$	Water, R-134a	$h_{tp} = 436.48 Bo_{ch}^{0.522} We_{ch}^{0.351} X_{vt}^{0.665} h_{sp,ch}$ $Bo_{ch} = \frac{q''_w}{G_{av}h_{FG}}$, $We_{ch} = \frac{G_{av}^2 d_h}{\sigma \rho_F}$, $X_{vt} = \left(\frac{f_f Re_G^{0.25}}{0.079}\right)^{0.5}\left(\frac{1-x}{x}\right)^{0.5}\left(\frac{\rho_G}{\rho_L}\right)^{0.5}$ for developing flow $Nu_{ch} = 0.775\left[24\left(1 - 1.355\beta + 1.947\beta^2 - 1.701\beta^3 + 0.953\beta^4 - 0.254\beta^5\right)\right]^{1/3}[L/(d_h Re \mathrm{Pr})]^{-1/3}$ for fully developed flow $Nu_{ch} = 8.235\left(1 - 2.042\beta + 3.085\beta^2 - 2.477\beta^3 + 1.058\beta^4 - 0.186\beta^5\right)$ $f_f = \frac{24}{Re_{ch}}\left(1 - 1.355\beta + 1.947\beta^2 - 1.701\beta^3 + 0.953\beta^4 - 0.254\beta^5\right)$ $h_{sp,ch} = \mathrm{Cor}\frac{Nu_{ch}k_F}{d_h}$, $\mathrm{Cor} = \frac{1 - 1.883\beta + 3.767\beta^2 - 5.814\beta^3 + 5.361\beta^4 - 2.0\beta^5}{1 - 2.042\beta + 3.085\beta^2 - 2.477\beta^3 + 1.058\beta^4 - 0.186\beta^5}$
7	Koşar et al. [21]	Rectangular, microchannels, 264 μm × 200 μm, $L = 0.01$ m, $G_{av} = 41$–302 kg/m^2 s, $0 < x_e < 0.9$	Water	Nucleate boiling: $h_{tp} = 1.068(q'')^{0.64}$ Convective boiling: $h_{tp} = 4.068 \times 10^4 (Re_{LO})^{0.12}(1 - x_e)^{0.8}\left(\frac{1-x_e}{x_e}\right)^{0.02}$

5.2. Comparison with existing correlations and development of boiling correlations

The two-phase heat transfer coefficients obtained in the current study are compared with five published correlations, two new (developed through the results of this study) empirical correlations and a correlation developed for plain microchannels (Table 2). As seen from Fig. 8, the predictions of the existing correlations developed for conventional tube bundles are not in good agreement with the experimental results. The correlations of Hwang and Yao [78] and Dowlati et al. [86] underpredict all the experimental data, while Hsu [80], Gupta et al. [84] and Gupta [89] correlations overpredict most of experimental data. The predictions are better for lower qualities ($x < 0.4$) and deteriorate at higher qualities. It is commonly accepted that no generally applicable correlation is available which is capable of predicting heat transfer coefficient over a large range of forced convection thermal-hydraulic conditions and bundle configurations [80,81]. Therefore, the large deviation between available correlations and the current results is not completely surprising. Furthermore, several important differences between the current configuration and the available correlations exist: (a) most large scale correlations are developed for circular tubes in cross-flow boiling, (b) the pin fins in the current heat sink have relatively small H/D ratio ($H/D = 2.43$) unlike the long tubes ($H/D > 8$) in conventional tube bundles, and (c) the range of mass qualities in the literature is not as broad as in the current study. All these differences result in a significant deviation between the predictions of existing correlations and the current experimental data.

Lee and Mudawar correlation [24] and the correlation developed by Koşar et al. [21] are included in Table 2 in order to evaluate whether correlations developed for microscale are capable of predicting experimental data obtained from a different configuration but in a similar length scale. The Reynolds, Nusselt and Boiling numbers were reevaluated according to the dimensions of the channel (based on the hydraulic diameter, $d_h = 328$ μm). Two methods to be implemented in Lee and Mudawar correlation [24] were used to calculate the single-phase heat transfer coefficient; one assumed the flow to be fully developed and the other to be developing flow. The Martinelli parameter corresponding to laminar fluid flow and turbulent gas flow was selected. Because the Martinelli parameter approaches to infinity as $x \to 0$, the average quality ($x_e/2$) was used in obtaining X_{vt}. The results for low exit qualities ($x_e/2 < 0.05$) were excluded in the comparison, since a different expression was recommended by Lee and Mudawar [24] for qualities below 0.05. With developing flow assumption, the correlation did not predict the experimental data well (MAE = 113%) as shown in Fig. 8f. However, when fully developed flow is assumed, a significant improvement in the prediction was observed as seen in Fig. 8g. Although the correlation trend does not concur with the experimental trend, overall it resulted in an acceptable prediction with MAE of 29.8%. The correlation of Koşar et al. [21] underpredicts the experimental data, which corresponds to nucleate boiling, while it provides a fair prediction to the data designated as convective boiling dominant with MAE of 37.6% (Fig. 8h). However, similar to the Lee and Mudawar correlation [24] it did not follow the trend of the experimental data. These findings may suggest that size scale effects are considerably more important than configuration effects at least when scaling from conventional scale to microscale.

The scatter and inability of existing large scale correlations to predict the heat transfer coefficient suggest that existing correlations are inadequate in predicting boiling heat transfer for the current micro pin fin heat sink. In an attempt to correlate the experimental data two different correlations were examined:

$$\begin{aligned} &\bar{h}_{tp} = a_1 q''^{a_2}_w + a_3 \bar{h}^{a_4}_{sp} \\ &\text{where} \\ &a_1 = \tfrac{3.42\times10^7}{G^{1.16} h^{1.16}_{FG}}, \quad a_2 = 1.01, \\ &a_3 = 0.12, \quad a_4 = 0.7 \\ &\quad \text{MAE} = 26.1\% \text{ (correlation 8)} \end{aligned} \tag{16}$$

$$\begin{aligned} &\bar{h}_{tp} = b_1 Re^{b_2}_{Lo} (1 - x_e)^{b_3} \left(\tfrac{1-x_e}{x_e}\right)^{b_4} \\ &b_1 = 819, \quad b_2 = 0.6, \\ &b_3 = 0.22, \quad b_4 = 0.01 \\ &\quad \text{MAE} = 14\% \text{ (correlation 9)} \end{aligned} \tag{17}$$

The constants a_1, a_2, a_3, a_4, b_1, b_2, b_3 and b_4 in the above equations were obtained through the least squares method. The first correlation is a Chen-type correlation and has a similar form to the one used by Gupta et al. [84]. The second correlation was adapted from correlations developed for microchannels (e.g., [18] (convective boiling part), [21]) and assumes convective boiling heat transfer mechanism. The single-phase heat transfer coefficient was calculated from Eq. (12), and the Reynolds number was evaluated assuming the liquid to flow alone in the pin fin bundle at saturation conditions. Since correlation 8 results in monotonically increasing heat transfer coefficients with heat flux and correlation 9 provides declining values with quality, correlation 8 was used to predict heat transfer coefficient at low mass qualities (for qualities corresponding to increasing heat transfer coefficients with quality), while correlation 9 was employed for prediction at high mass qualities (when the heat transfer coefficient decreases with quality). Furthermore, correlation 8 strongly depends on the Boiling number, which is a key parameter during nucleate boiling, according to conventional scale knowledge; the second correlation depends on the mass quality, which affects the heat transfer coefficient for convective boiling.

Based on the characteristic trend of the heat transfer coefficient and similar to Koşar et al. [21] a map segregating the boiling mechanisms was developed (Fig. 9) as a function of the Boiling and Reynolds numbers. The region corresponding to the increasing heat transfer coefficient

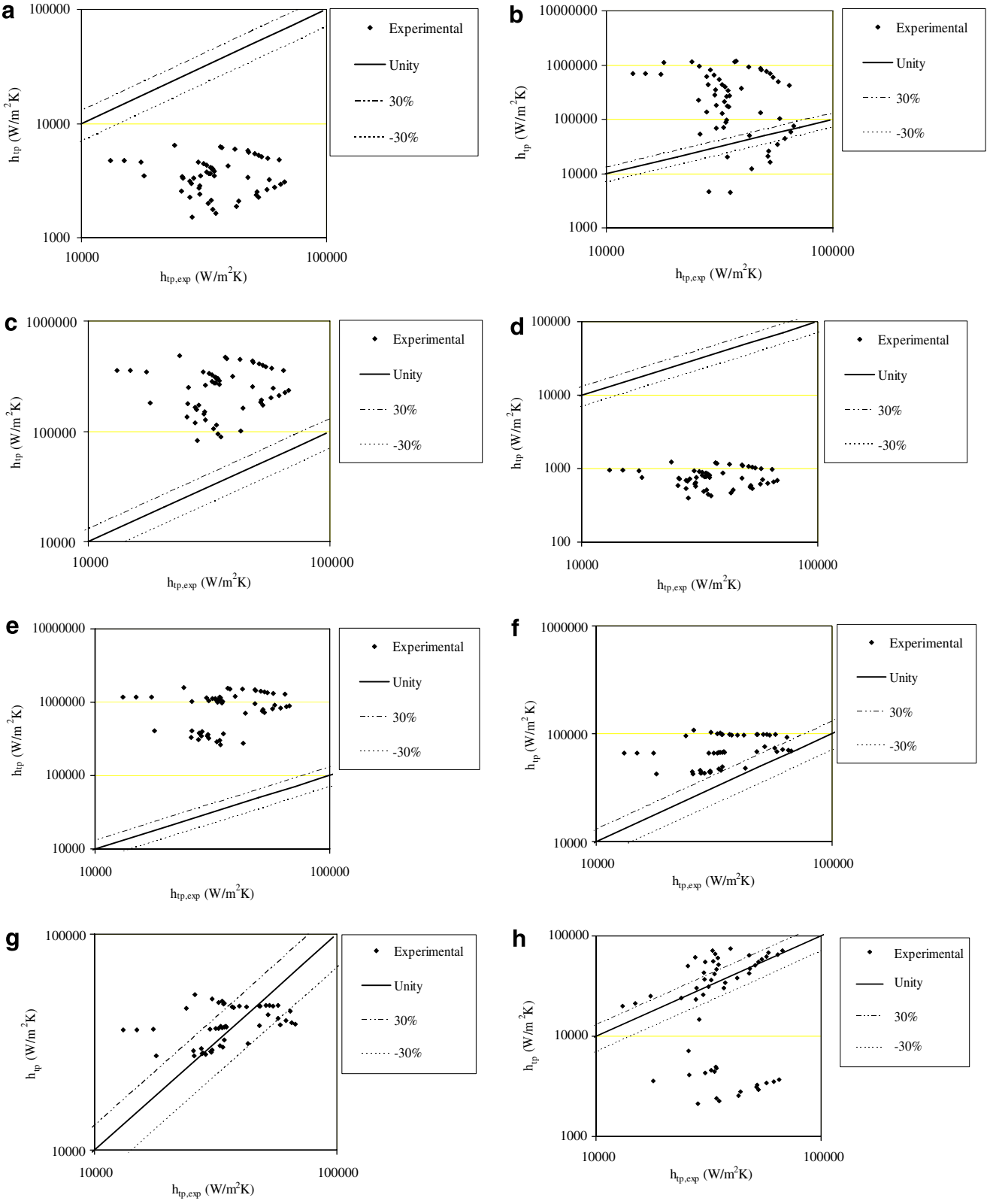

Fig. 8. Two-phase heat transfer coefficient comparison with the existing correlations. Correlations 1–3: (a) Hwang and Yao [78], (b) Hsu [80], (c) Gupta et al. [84]. Correlations 4 and 5: (d) Dowlati et al. [86], (e) Gupta [89]. Correlations 6 and 7: (f) Lee and Mudawar [24] (developing flow approach); (g) Lee and Mudawar [24] (fully developed flow approach). (h) Koşar et al. [21].

was considered to be dominated by nucleate boiling, while the region characterized by decreasing values was assumed to be convective boiling dominant. As seen from Fig. 9, the Boiling number is the dominant parameter in dictating the

heat transfer mechanism, while the Reynolds number is less important as evident by the steep transition curve segregating nucleate and convective boiling. It should be noted that other dimensionless parameters, such as the Weber or Capillary numbers, might be of significant importance, and should provide additional insight to the boiling mechanisms. However, experiments have been performed with R-123, and currently, insufficient data are available to propose reliable transition boundaries accounting for such potential dimensionless parameters.

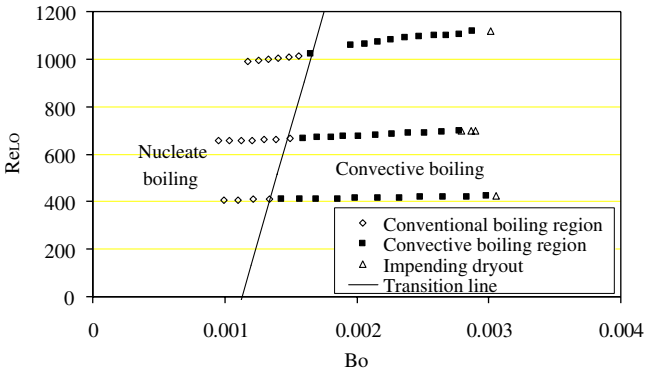

Fig. 9. Boiling map constructed based on the trend in experimental two-phase heat transfer coefficients.

5.3. Flow patterns

Similar to flow boiling in conventional scale tube bundles, bubbly, wavy intermittent, and spray-annular flow patterns were identified depending on the heat flux and mass velocity (Fig. 10). At low Boiling numbers, bubbly flow in which small bubbles are surrounded by a liquid phase is observed (Fig. 10a). For intermediate Boiling numbers, a thick liquid layer surrounds the micro pin fins and has a wavy interface with the vapor phase which contains liquid spray (Fig. 10b). At higher Boiling numbers, the primary flow pattern is spray-annular, which is distinguished by dark thin liquid layers surrounding the surface of the micro pin fins and large volumes of vapor phase with liquid spray (Fig. 10c), and is also present at CHF condition.

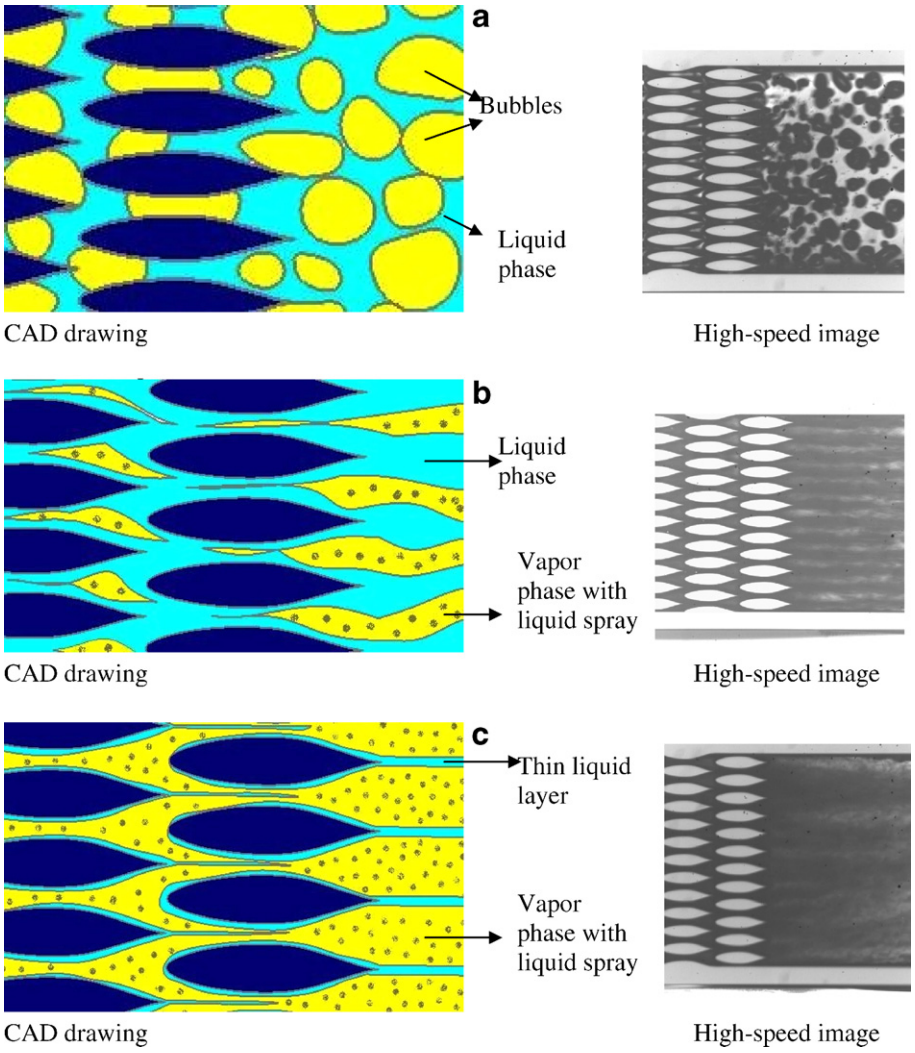

Fig. 10. Flow patterns: (a) bubbly flow, (b) wavy intermittent flow, (c) spray annular flow.

Fig. 11a displays a flow map including the boundaries between each flow pattern based on the Reynolds and Boiling numbers. Comparing Figs. 9 and 11a, it can be seen that the bubbly and wavy intermittent flow regimes are closely related to nucleate boiling heat transfer, while the spray annular flow morphologies correlate well with convective boiling. This is not surprising, and the linkage between flow patterns and heat transfer mechanisms is well documented in numerous archival publications [12,14,18, 19,21,22,106].

In many archival reports flow maps are often expressed in terms of hydrodynamic variables like superficial phase velocity. Accordingly, the flow map is also presented using the superficial velocities in Fig. 11b. Low vapor superficial velocities and high liquid superficial velocities correspond to bubbly flow, while high vapor superficial velocities are associated with spray-annular flow. The difference in the current flow map from the existing general flow map developed by Noghrehkar et al. [100] is that the spray-annular flow pattern is evident in a larger portion of the flow map in the current study. In their flow map, however, the spray-annular flow pattern was confined to low liquid superficial velocities ($j_L < 0.2$ m/s). This can be linked to high mass velocities in the current studies ($G > 900$ kg/m^2 s). Noghrehkar et al. [100] operated at mass velocities up to 750 kg/m^2 s, whereas the lowest mass velocity in the current study is 976 kg/m^2 s. As seen from Fig. 11b, the liquid superficial velocity shifts to a lower value for spray-annular flow with diminishing mass velocity. Thus, for low mass velocities, liquid superficial velocities under

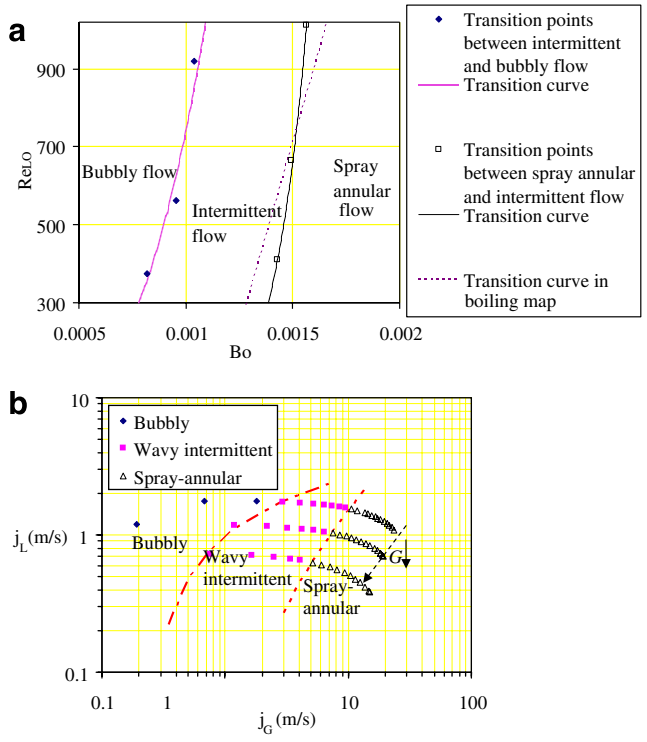

Fig. 11. (a) Flow map demonstrating the flow patterns and their transition points and curves along with the transition curve in boiling map (Fig. 8). (b) Flow map based on superficial velocities.

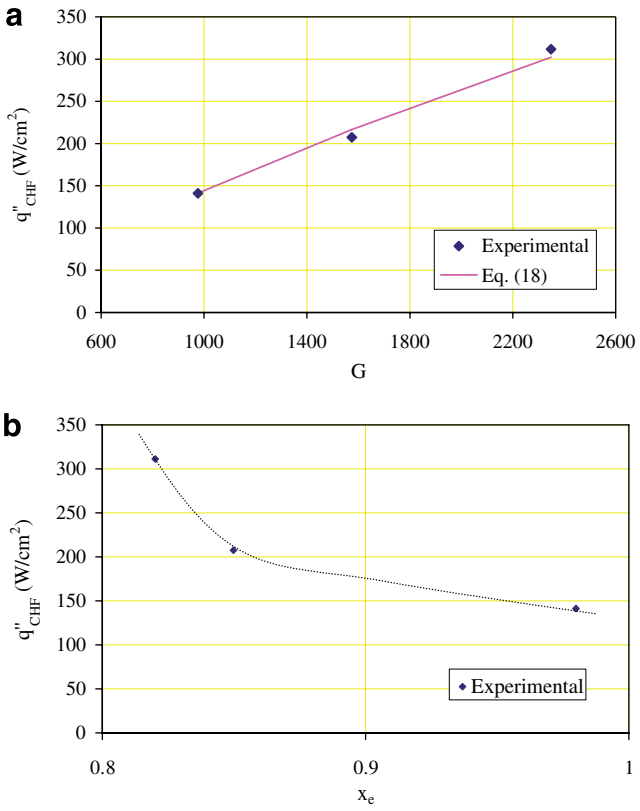

Fig. 12. Critical heat flux as a function of (a) G and (b) x_e.

spray-annular flow are more consistent with the flow map of Noghrehkar et al. [100].

5.4. Critical heat flux

As shown in Fig. 12a and b, the dependency of CHF on the mass velocity and heat flux is considerable, and is in accordance with conventional scale correlations trends [92–94,109–114]. That is, CHF increases with G and decreases with x_e. The existence of annular flow together with high mass quality prior to CHF condition implies that dryout mechanism triggers CHF condition. The high qualities at CHF conditions also support this claim when referring to the map of Leroux and Jensen [93]. A high mass velocity-type CHF correlation recommended for annular flow proposed by Katto and Haramura [110], which was used to correlate experimental CHF data in mini-/microchannels [21,112–114], was employed to fit the CHF data

$$q''_{CHF} = 0.0011 G h_{FG} We^{-0.04} \quad (18)$$

The correlation provides excellent prediction of the data with MAE of 2.6%. This suggests that a microchannel type correlation can successfully predict CHF in micro pin fin heat sinks.

6. Conclusions

In this study, flow boiling heat transfer experiments have been conducted in a hydrofoil based micro pin fin

heat sink. Governing heat transfer mechanisms have been identified for different operating conditions. A heat transfer mechanism map, as well as a flow map containing the experimental data, has been developed. The main conclusions drawn from this study are:

- The heat transfer coefficient increases with heat flux, attains a maximum and then monotonically declines until the CHF condition is reached.
- The increasing trend of the experimental data at low qualities is associated with nucleate boiling dominant heat transfer mechanism, whereas the continuous decline with heat flux at higher qualities is linked with convective boiling dominant heat transfer mechanism.
- Existing large scale correlations provided large scatter and inability to predict the heat transfer coefficients, but microchannel correlations provide a more reasonable agreement with the current experimental data. More research should be conducted to develop better prediction tools.
- Based on the characteristic trend of the heat transfer coefficient, a map segregating the boiling mechanisms was developed. The Boiling number is found to be the dominant parameter in detecting the boiling mechanism.
- Bubbly, wavy intermittent, and spray-annular flow patterns were identified depending on the heat flux and mass velocity, and a flow map was constructed to specify the transition boundaries between each flow pattern.
- CHF increases with mass velocity and decreases with mass quality, which is in agreement with available literature, and the dryout mechanism triggers the CHF condition.

Acknowledgements

This work was supported by the Office of Naval Research through the Ships and Engineering Systems Division, Code 331 (Program Officer: Dr. Mailc Spector). The microfabrication was performed in part at the Cornell NanoScale Facility (a member of the National Nanotechnology Infrastructure Network) which is supported by the National Science Foundation under Grant ECS-0335765, its users, Cornell University and industrial affiliates. The authors are thankful to Mr. Chandan Mishra and Mr. Brandon Schneider for their valuable suggestions during the development of the CAD model.

References

[1] T.S. Ravigururajan, M.K. Drost, Single-phase flow thermal performance characteristics of a parallel microchannel heat exchanger, J. Enhanced Heat Transfer 6 (5) (1999) 383–393.
[2] S.S. Mehendale, A.M. Jacobi, R.K. Shah, Fluid flow and heat transfer at micro- and meso-scales with application to heat exchanger design, Appl. Mech. Rev. 53 (7) (2000) 175–193.
[3] G.P. Celata, M. Cumo, G. Zummo, Thermal-hydraulic characteristics of single-phase flow in capillary pipes, Exp. Therm. Fluid Sci. 28 (2–3) (2004) 87–95.
[4] S.V. Garimella, V. Singhal, Single-phase flow and heat transport and pumping considerations in microchannel heat sinks, Heat Transfer Eng. 25 (1) (2004) 15–25.
[5] S.G. Kandlikar, W.J. Grande, Evaluation of single-phase flow in microchannels for high heat flux chip cooling – thermohydraulic performance enhancement and fabrication technology, J. Heat Transfer Eng. 25 (8) (2004) 5–16.
[6] J. Li, G.P. Peterson, P. Cheng, Three-dimensional analysis of heat transfer in a micro-heat sink with single-phase flow, Int. J. Heat Mass Transfer 47 (19–20) (2004) 4215–4231.
[7] W. Owhaib, B. Palm, Experimental investigation of single-phase convective heat transfer in circular microchannels, Exp. Therm. Fluid Sci. 28 (2–3) (2004) 105–110.
[8] P.S. Lee, S.V. Garimella, D. Liu, Investigation of heat transfer in rectangular microchannels, Int. J. Heat Mass Transfer 48 (9) (2005) 1688–1704.
[9] D. Pinjala, T.N. Wong, K.C. Toh, Y.K. Joshi, Single-phase liquid cooled microchannel heat sink for electronic packages, Appl. Therm. Eng. 25 (10) (2005) 1472–1487.
[10] Q.X. Wang, C. Yap, A.S. Majumdar, Effects of two-dimensional roughness in flow in microchannels, J. Electron. Packaging 127 (2005) 357–361.
[11] L. Jiang, M. Wong, Y. Zohar, Forced convection boiling in microchannel heat sink, J. Microelectromech. Syst. 10 (1) (2001) 80–87.
[12] S.G. Kandlikar, Two-phase flow patterns, pressure drop, and heat transfer during boiling in minichannels flow passages of compact evaporators, Heat Transfer Eng. 23 (1) (2002) 5–23.
[13] G.R. Warrier, V.K. Dhir, L.A. Momoda, Heat transfer and pressure drop in narrow rectangular channel, Exp. Therm. Fluid Sci. 26 (2002) 53–64.
[14] W. Qu, I. Mudawar, Flow boiling heat transfer in two-phase microchannel heat sink: I. Experimental investigation and assessment of correlation methods, Int. J. Heat Mass Transfer 46 (15) (2003) 2755–2771.
[15] H.Y. Wu, P. Cheng, Visualization and measurements of periodic boiling in silicon microchannels, Int. J. Heat Mass Transfer 46 (14) (2003) 2603–2614.
[16] P.C. Lee, F.G. Tseng, C. Pan, Bubble dynamics in microchannels. Part I: single microchannel, Int. J. Heat Mass Transfer 47 (25) (2004) 5575–5589.
[17] W. Owhaib, C. Martín-Callizo, B. Palm, Evaporative heat transfer in vertical circular microchannels, Appl. Therm. Eng. 24 (2004) 1241–1253.
[18] M.E. Steinke, S.G. Kandlikar, An experimental investigation of flow boiling characteristics of water in parallel microchannels, J. Heat Transfer 126 (4) (2004) 518–526.
[19] J.R. Thome, Boiling in micro channels: a review of experiment and theory, Int. J. Heat Fluid Flow 25 (2004) 128–139.
[20] J.-M. Koo, S. Im, L. Jiang, K.E. Goodson, Integrated microchannel cooling for three-dimensional electronic circuit architectures, J. Heat Transfer 127 (1) (2005) 49–58.
[21] A. Koşar, C.J. Kuo, Y. Peles, Boiling heat transfer in rectangular microchannels with reentrant cavities, Int. J. Heat Mass Transfer 48 (23) (2005) 4867–4886.
[22] A. Koşar, C.J. Kuo, Y. Peles, Reduced pressure boiling heat transfer in rectangular microchannels with interconnected reentrant cavities, J. Heat Transfer 127 (10) (2005) 1106–1114.
[23] A. Koşar, C.J. Kuo, Y. Peles, Suppression of boiling flow oscillations in parallel microchannels by inlet restrictors, J. Heat Transfer 128 (3) (2006) 251–260.
[24] J. Lee, I. Mudawar, Two-phase flow in high-heat-flux micro-channel heat sink for refrigeration cooling applications: part II—Heat transfer characteristics, Int. J. Heat Mass Transfer 48 (5) (2005) 941–955.

[25] L. Zhang, E.N. Wang, K.E. Goodson, T.W. Kenny, Phase change phenomena in silicon microchannels, Int. J. Heat Mass Transfer 48 (8) (2005) 1572–1582.
[26] C.J. Kuo, A. Koşar, Y. Peles, S. Virost, C. Mishra, M.K. Jensen, Bubble dynamics during boiling in enhanced surface microchannels, J. Microelectromechan. Syst., in press.
[27] C.J. Kuo, A. Koşar, M.K. Jensen, Y. Peles, Boiling in enhanced surface microchannels, in: ASME International Mechanical Engineering Congress and Exposition, November 5–12, Orlando, FL, IMECE2005-80412, 2005.
[28] B. Schneider, Y. Peles, Hydrodynamic cavitation and boiling in refrigerant (R-123) flow inside microchannels, Int. J. Heat Mass Transfer, in review.
[29] A. Koşar, Y. Peles, Thermal-hydraulic performance of MEMS-based pin fin heat sink, J. Heat Transfer 128 (2) (2006) 121–131.
[30] Y. Peles, C.J. Kuo, A. Koşar, C. Mishra, B. Schneider, Forced convective heat transfer across a pin fin micro heat exchanger, Int. J. Heat Mass Transfer 48 (17) (2005) 3615–3627.
[31] A. Koşar, C. Mishra, Y. Peles, Laminar flow across a bank of low aspect ratio micro pin fins, J. Fluids Eng. 127 (3) (2005) 419–430.
[32] E.G. Colgan, B. Furman, M. Gaynes, W. Graham, N. LaBianca, J.H. Magerlein, R.J. Polastre, M.B. Rothwell, R.J. Bezama, R. Choudhary, K. Marston, H. Toy, J. Wakil, J. Zitz, R. Schmidt, A practical implementation of silicon microchannel coolers for high power chips, in: 21st IEEE SEMI-THERM Symposium, San Jose, CA, March 15–17, 2005.
[33] R.S. Prasher, J. Dirner, J.-Y. Chang, A. Myers, D. Chau, D. He, S. Prstic, Nusselt number and friction factor of staggered arrays of low aspect ratio micro pin fins under cross flow, J. Heat Transfer, in press.
[34] W. Qu, F. Pfefferkorn, Y. Jeon, Experimental study of single-phase flow and heat transfer in micro-pin-fin and micro-channel heat sinks, in: ASME International Mechanical Engineering Congress and Exposition, November 5–12, Orlando, FL, IMECE2005-80557, 2005.
[35] A. Koşar, Y. Peles, Convective flow of refrigerant (R-123) across a bank of micro pin fins, Int. J. Heat Mass Transfer 49 (2006) 3142–3155.
[36] A.A. Zukauskas, Heat transfer from tubes in cross flow, Advances in Heat Transfer, vol. 8, Academic Press, New York, 1972, pp. 93–160.
[37] S. Whitaker, Forced convection heat-transfer correlations for flow in pipes, past flat plates, single cylinders, single spheres, and for flow in packed-beds and tube bundles, AIChE J. 18 (2) (1972) 361–371.
[38] M.K. Chyu, Y.C. Hsing, V. Natarajan, Convective heat transfer of cubic fin arrays in a narrow channel, J. Heat Transfer 120 (1998) 362–367.
[39] E.M. Sparrow, V.B. Grannis, Pressure drop characteristics of heat exchangers consisting of arrays of diamond-shaped pin fins, Int. J. Heat Mass Transfer 34 (3) (1991) 589–600.
[40] T. Igarashi, Fluid flow and heat transfer around rectangular cylinders (the case of a width/height ratio of a section of 0.33–1.5), Int. J. Heat Mass Transfer 30 (1987) 893–901.
[41] J. Taborek, Shell-and-tube heat exchangers: single phase flowHandbook of Heat Exchanger Design, Hemisphere, New York, 1983 (Chapter 3.3).
[42] Y. Peng, Heat transfer and friction loss characteristics of pin fin cooling configurations, ASME J. Eng. Gas Turbines Power 106 (1984) 246–251.
[43] E.M. Sparrow, S.S. Kang, Longitudinally-finned cross flow tube banks and their heat transfer and pressure drop characteristics, Int. J. Heat Mass Transfer 28 (2) (1985) 339–350.
[44] J. Armstrong, D. Winstanley, A review of staggered array pin fin heat transfer for turbine cooling applications, ASME J. Turbomach. 110 (1988) 94–103.
[45] S.V. Garimella, Heat transfer and flow fields in confined jet impingement, Ann. Rev. Heat Transfer (1999) 413–494 (Chapter 7).
[46] L.A. Brignoni, S.V. Garimella, Heat transfer from a finned surface inducted air jet suction and impingement, J. Electron. Packaging 122 (2000) 282–285.
[47] H.A. El-Sheikh, S.V. Garimella, Heat transfer from pin fin heat sinks under multiple impinging jets, IEEE Trans. Adv. Packaging 23 (1) (2000) 113–120.
[48] H.A. El-Sheikh, S.V. Garimella, Enhancement of air jet impingement heat transfer using pin fin heat sinks, IEEE Trans. Compon. Packaging Technol. 23 (2) (2000) 300–308.
[49] C.-Y. Li, S.V. Garimella, Prandtl number effects and generalized correlations for confined and submerged jet impingement, Int. J. Heat Mass Transfer 44 (2001) 3471–3480.
[50] K.A. Moores, Y.K. Joshi, G.H. Schiroky, Thermal characterization of a liquid cooled Al–Sic base plate with integral pin fins, IEEE Trans. Compon. Packaging Technol. 24 (2) (2001) 213–219.
[51] E. Yu, Y.K. Joshi, Heat transfer enhancement from enclosed discrete components using pin-fin heat sinks, Int. J. Heat Mass Transfer 45 (25) (2002) 4957–4966.
[52] K.A. Moores, Y.K. Joshi, Effect of tip clearance on the thermal and hydrodynamic performance of a shrouded pin fin array, J. Heat Transfer 125 (2003) 999–1006.
[53] O.N. Şara, Performance analysis of rectangular ducts with staggered square pin fins, Energy Conserv. Manage. 144 (2003) 1787–1803.
[54] D. Kim, S.J. Kim, A. Ortega, Compact modeling of fluid flow and heat transfer in pin fin heat sinks, J. Electron. Packaging 126 (2004) 342–350.
[55] B.E. Short Jr., D.C. Price, P.E. Raad, Design of cast pin fin coldwalls for air-cooled electronic systems, J. Electron. Packaging 126 (2004) 67–73.
[56] M.B. Doğruöz, M. Urdaneta, A. Ortega, Experiments and modeling of the hydraulic resistance and heat transfer of in-line square pin fin heat sinks with top by-pass flow, Int. J. Heat Mass Transfer 48 (2005) 5058–5071.
[57] F. Gori, M. Borgia, A.D. Altan, I. Petracci, Cooling of a finned cylinder by a jet flow of air, J. Heat Transfer 127 (2005) 1416–1421.
[58] K.W. Haley, J.W. Westwater, Boiling heat transfer from single fins, in: 3rd International Heat Transfer Conference, AIChE, Chicago, 1966, pp. 245–253.
[59] F.S. Lai, Y.Y. Hsu, Temperature distribution in a fin partially cooled by nucleate boiling, AIChE J. 13 (1967) 817–822.
[60] D.R. Cash, G.J. Klein, J.W. Westwater, Approximate optimum fin design for boiling heat transfer, J. Heat Transfer 93 (1971) 19–24.
[61] H.C. Ünal, An analytic study of boiling heat transfer from a fin, Int. J. Heat Mass Transfer 30 (2) (1987) 341–349.
[62] R.L. Webb, C. Osais, Nucleate pool boiling data for five refrigerants on plain, integral-fin and enhanced tube geometries, Int. J. Heat Mass Transfer 35 (1992) 893–1904.
[63] S.S. Hsien, P.T. Hsu, Nucleate boiling characteristics for R-14, distilled water and R-134a on plain and rib-roughened tube geometries, Int. J. Heat Mass Transfer 37 (1994) 1423–1432.
[64] S.P. Liaw, R.H. Yeh, Fins with temperature dependent surface heat flux-II. Multi-boiling heat transfer single heat transfer, Int. J. Heat Mass Transfer 37 (10) (1994) 1517–1524.
[65] L.H. Chien, R.L. Webb, A nucleate boiling model for structured enhanced surfaces, Int. J. Heat Mass Transfer 41 (14) (1998) 2183–2195.
[66] W.W. Lin, J.C. Yang, D.J. Lee, Metastable pin fin boiling, Int. J. Heat Mass Transfer 43 (2000) 1629–1635.
[67] K.N. Rainey, S.M. You, Pool boiling heat transfer from plain microporous, square pin-finned surfaces in saturated FC-72, J. Heat Transfer 122 (2000) 509–516.
[68] L.H. Chien, R.L. Webb, Effect of geometry and fluid property parameters on performance of tunnel and pore enhanced boiling surfaces, J. Enhanced Heat Transfer 8 (5) (2001) 329–339.
[69] G. Guglielmini, M. Misale, C. Schenone, Boiling of saturated FC-72 on square pin fin arrays, Int. J. Therm. Sci. 46 (2002) 599–608.
[70] K.N. Rainey, S.M. You, S. Lee, Effect of pressure, subcooling, and dissolved gas on pool boiling heat transfer from microporous,

square pin-finned surfaces in FC-72, Int. J. Heat Mass Transfer 46 (2003) 23–35.
[71] L.H. Chien, C.C. Chang, Enhancement of pool boiling on structured surfaces using HFC-4310 and water, J. Enhanced Heat Transfer 11 (1) (2004) 23–32.
[72] Z.H. Liu, Y.-H. Qiu, Boiling characteristics of R-11 in compact tube bundles with smooth and enhanced tubes, Exp. Heat Transfer 17 (2004) 91–102.
[73] S.P. Liaw, R.-H. Yeh, W.-T. Yeh, A simple design of fins for boiling heat transfer, Int. J. Heat Mass Transfer 48 (13) (2005) 2493–2502.
[74] H. Honda, H. Takamatsu, J.J. Wei, Enhanced boiling of FC-72 on silicon chips with micro-pin-fins and submicron-scale roughness, J. Heat Transfer 124 (2002) 383–390.
[75] H. Honda, H. Takamatsu, J.J. Wei, Effect of size of micro-pin-fin on boiling heat transfer from silicon chips immersed in FC-72, in: Proceedings of 12th International Heat Transfer Conference, 2002, pp. 75–80.
[76] H. Honda, J.J. Wei, Enhanced boiling heat transfer from electronic components by use of surface microstructures, Exp. Therm. Fluid Sci. 28 (2004) 159–169.
[77] R. Dowlati, M. Kawaji, Two-phase flow and boiling heat transfer in tube bundles, Handbook of Phase Change: Boiling and Condensation, Taylor& Francis, Ann Arbor, 1999 (Chapter 12).
[78] T.H. Hwang, S.C. Yao, Cross flow heat transfer in tube bundles at low Reynolds numbers, J. Heat Transfer 108 (1986) 697–700.
[79] K. Cornwell, The influence of bubbly flow on boiling from a tube in a bundle, Int. J. Heat Mass Transfer 33 (12) (1990) 2579–2584.
[80] J.-T. Hsu, A parametric study of boiling heat transfer in a horizontal tube bundle, Ph.D. Dissertation, University of Wisconsin-Milwaukee, Milwaukee, WI, 1987.
[81] M.K. Jensen, J.-T. Hsu, A parametric study of boiling heat transfer in a horizontal tube bundle, J. Heat Transfer 110 (1988) 976–981.
[82] G.D. Mandrusiak, V.P. Carey, Convective boiling in vertical channels with different offset strip fin geometries, J. Heat Transfer 111 (1989) 697–700.
[83] G.D. McGills, V.P. Carey, Subcooled convective boiling of binary-mixtures over an array of heated elements, J. Thermophys. Heat Transfer 7 (2) (1993) 346–351.
[84] A. Gupta, J.S. Saini, H.K. Varma, Boiling heat transfer in small horizontal tube bundles at low cross-flow velocities, Int. J. Heat Mass Transfer 38 (4) (1995) 599–605.
[85] D. Copeland, Single-phase and boiling cooling of small pin fin arrays by multiple nozzle jet impingement, J. Electron. Packaging 118 (1) (1996) 21–26.
[86] R. Dowlati, M. Kawaji, A.M.C. Chan, Two-phase crossflow and boiling heat transfer in horizontal tube bundles, J. Heat Transfer 118 (1996) 124–131.
[87] L.-D. Huang, L.C. Witte, Highly subcooled boiling in crossflow, J. Heat Transfer 123 (2001) 1080–1085.
[88] N.-H. Kim, J.-P. Cho, B. Youn, Forced convective boiling of pure refrigerants in a bundle of enhanced tubes having pores and connecting gaps, Int. J. Heat Mass Transfer 45 (2002) 2449–2463.
[89] A. Gupta, Enhancement of boiling heat transfer in a 5×3 tube bundle, Int. J. Heat Mass Transfer 48 (2005) 3763–3772.
[90] S.C. Yao, T.H. Hwang, Critical heat flux on horizontal tubes in an upward crossflow of Freon-113, Int. J. Heat Mass Transfer 32 (1) (1989) 95–103.
[91] G.D. McGills, V.P. Carey, B.D. Strom, Geometry-effects on critical heat-flux for subcooled convective boiling from an array of heated elements, J. Heat Transfer 113 (2) (1991) 463–471.
[92] S. Dykas, M.K. Jensen, Critical heat flux on a tube in a horizontal tube bundle, Exp. Therm. Fluid Sci. 5 (1992) 34–39.
[93] K.M. Leroux, M.K. Jensen, Critical heat flux in horizontal tube bundles in vertical crossflow of R-113, J. Heat Transfer 114 (1992) 79–184.
[94] M.K. Jensen, H. Tang, Correlations for the CHF condition in two-phase crossflow through multitube bundles, J. Heat Transfer 116 (1994) 780–783.
[95] K. Ishihara, J.W. Palen, J. Taborek, Critical review of correlations for predicting two-phase flow pressure drop across tube banks, Heat Transfer Eng. 1 (1980) 23–32.
[96] G.D. Mandrusiak, V.P. Carey, Pressure-drop characteristics of 2-phase flow in a vertical channel with offset strip fins, Exp. Therm. Fluid Sci. 1 (1988) 41–50.
[97] D.S. Schrage, J.T. Hsu, M.K. Jensen, Two-phase pressure drop in vertical crossflow across a horizontal tube bundle, Am. Inst. Chem. Eng. J. 34 (1988) 107–115.
[98] G.P. Xu, K.W. Tou, C.P. Tso, Two-phase void fraction and pressure drop in horizontal cross flow across a tube bundle, J. Fluids Eng. 120 (1998) 140–145.
[99] I.D.R. Grant, D. Chisholm, Two-phase flow on the shell-side of a segmentally baffled shell-and-tube heat exchanger, J. Heat Transfer 101 (1979) 38–42.
[100] G.R. Noghrehkar, M. Kawaji, A.M.C. Chan, Investigation of two-phase flow regimes in tube bundles under cross-flow conditions, Int. J. Multiphase Flow 25 (1999) 857–874.
[101] S. Kline, F.A. McClintock, Describing uncertainties in single-sample experiments, Mech. Eng. 75 (1) (1953) 3–8.
[102] W.M. Rohsenow, A method of correlating heat transfer data for surface boiling of liquids, J. Heat Transfer 74 (1952) 969–976.
[103] J.C. Chen, A correlation for boiling heat transfer to saturated fluids in convective flows, Ind. Eng. Chem. Process Design Dev. 5 (1966) 322–329.
[104] K. Stephan, M. Abdelsalam, Heat transfer correlations for natural convection boiling, Int. J. Heat Mass Transfer 23 (1) (1980) 73–87.
[105] G.M. Lazarek, S.H. Black, Evaporative heat transfer, pressure drop and critical heat flux in a small diameter vertical tube with R-113, Int. J. Heat Mass Transfer 25 (7) (1982) 945–960.
[106] K. Cornwell, P.A. Kew, Boiling in small parallel channels, Energy Efficiency Process Technol. 37 (2) (1992) 624–638.
[107] T.N. Tran, M.W. Wambsganns, D.M. France, Small circular-and rectangular-channel boiling with two refrigerants, Int. J. Multiphase Flow 22 (3) (1996) 485–498.
[108] Z.Y. Bao, D.F. Fletcher, B.S. Haynes, Flow boiling heat transfer of Freon R11 and HCFC123 in narrow passages, Int. J. Heat Mass Transfer 43 (18) (2000) 3347–3358.
[109] R.W. Bowring, A simple but accurate round tube uniform heat flux, dryout correlation over the pressure range 0.7–17 MN/m^2 (100–2500 psia), Br. Report AEEW-R 789, Winfrith, UK, 1972.
[110] Y. Katto, Y. Haramura, Critical heat flux on a uniformly heated horizontal cylinder in an upward cross flow of saturated liquid, Int. J. Heat Mass Transfer 26 (1983) 199–1205.
[111] Y. Katto, H. Ohne, An improved version of the generalized correlation of critical heat flux for convection boiling in uniformly heated vertical tubes, Int. J. Heat Mass Transfer 27 (9) (1984) 1641–1648.
[112] C.N. Ammerman, W.M. You, Enhancing small-channel convective boiling performance using a microporous surface coating, J. Heat Transfer 123 (5) (2001) 976–983.
[113] M.B. Bowers, I. Mudawar, High flux boiling in low flow rate, low pressure drop mini-channel and micro-channel heat sinks, Int. J. Heat Mass Transfer 37 (2) (1994) 321–334.
[114] W. Qu, I. Mudawar, Measurement and correlation of critical heat flux in two-phase micro-channel heat sinks, Int. J. Heat Mass Transfer 47 (2004) 2045–2059.